J Seismol (2017) 21:193–208
DOI 10.1007/s10950-016-9597-1

ORIGINAL ARTICLE

Real-time envelope cross-correlation detector: application to induced seismicity in the Insheim and Landau deep geothermal reservoirs

Margarete Vasterling · Ulrich Wegler · Jan Becker · Andrea Brüstle · Monika Bischoff

Received: 6 February 2016 / Accepted: 22 June 2016 / Published online: 3 August 2016

Abstract We develop and test a real-time envelope cross-correlation detector for use in seismic response plans to mitigate hazard of induced seismicity. The incoming seismological data are cross-correlated in real-time with a set of previously recorded master events. For robustness against small changes in the earthquake source locations or in the focal mechanisms we cross-correlate the envelopes of the seismograms rather than the seismograms themselves. Two sequenced detection conditions are implemented: After passing a single trace cross-correlation condition, a network cross-correlation is calculated taking amplitude ratios between stations into account. Besides detecting the earthquake and assigning it to the respective reservoir, real-time magnitudes are important for seismic response plans. We estimate the magnitudes of induced microseismicity using the relative amplitudes between master event and detected event. The real-time detector is implemented as a SeisComP3 module. We carry out offline and online performance tests using seismic monitoring data of the Insheim and Landau geothermal power plants (Upper Rhine Graben, Germany), also including blasts from a nearby quarry. The comparison of the automatic real-time catalogue with a manually processed catalogue shows, that with the implemented parameters events are always correctly assigned to the respective reservoir (4 km distance between reservoirs) or the quarry (8 km and 10 km distance, respectively, from the reservoirs). The real-time catalogue achieves a magnitude of completeness around 0.0. Four per cent of the events assigned to the Insheim reservoir and zero per cent of the Landau events are misdetections. All wrong detections are local tectonic events, whereas none are caused by seismic noise.

Keywords Seismic monitoring · Induced seismicity · Real-time detector · Cross-correlation · Envelope · Geothermal energy

M. Vasterling (✉) · U. Wegler
Bundesanstalt für Geowissenschaften und Rohstoffe (BGR), Stilleweg 2, 30655 Hannover, Germany
e-mail: Margarete.Vasterling@bgr.de

J. Becker
Gempa GmbH, Telegrafenberg, 1447 Potsdam, Germany

A. Brüstle
Landesamt für Geologie und Bergbau Rheinland-Pfalz, Emy-Roeder-Strasse 5, 55129 Mainz, Germany

M. Bischoff
Formerly BGR, now Landesamt für Bergbau, Energie und Geologie, Stilleweg 2, 30655 Hannover, Germany

1 Introduction

Perceptible shaking related to waste water injection (Walsh and Zoback 2015; Weingarten et al. 2015) and hydraulic fracturing (Farahbod et al. 2015) from shale gas production in North America raised the public awareness of fluid induced seismicity. Felt

earthquakes also occurred when stimulating (e.g. Häring et al. 2008) or operating (e.g. Bönnemann et al. 2010) deep geothermal reservoirs. For mitigating induced seismic hazard, response plans define steps need to be taken (e.g. reduce injection pressure or flow rate) if predefined thresholds for e.g. magnitude, number of events or peak ground velocity (PGV) are exceeded (Bommer et al. 2006; Kraft et al. 2009). As the probability of larger events can be estimated from the number of smaller events by analysing the magnitude frequency distribution (Shapiro et al. 2007), it is essential to soundly detect small events, and distinct between induced events from the monitored reservoir and other events.

One challenge in densely populated Central Europe is, that geothermal power plants are often built near urban areas which impairs the signal quality of the local seismic network. Frequent transient noise bursts cause an unacceptable number of misdetections when using standard STA/LTA (Short Time Average over Long Time Average) triggers. Unlike STA/LTA triggers cross-correlation detectors take into account the full seismic signal, including the chronological sequence of the individual phases and their amplitude ratios when combining the whole seismic network. Schaff and Waldhauser (2010) found a reduction of the detection threshold by one order of magnitude with a very low rate of false detections from comparing a standard STA/LTA trigger and a correlation detector.

Cross-correlation methods are advantageous to find any kind of repeating or similar signal, providing a widespread spectrum of applications for seismology. It reaches from scanning global seismicity (Dodge and Walter 2015) or individual regions (e.g. Richards et al. 2006; Schaff and Richards 2011) for similar tectonic events to the monitoring of non volcanic tremors (Shelly et al. 2007), landslides (Chen et al. 2013), and the detection of aftershock sequences (Slinkard et al. 2013). It also includes the monitoring of induced seismicity at the stimulation and operation of geothermal reservoirs (Plenkers et al. 2013; Forghani-Arani et al. 2013), during hydraulic fracturing (Holland 2013; Song et al. 2010), and at waste water disposal sites (Skoumal et al. 2014) as well as from mining (Kubacki et al. 2014). Furthermore, Gibbons and Ringdal (2012) and Bobrov et al. (2014) evaluate the potential of cross-correlation detectors within the framework of the Comprehensive Nuclear-Test-Ban Treaty, e.g. for the detection of nuclear tests in North Korea.

Most detectors use the waveform data for cross-correlation with a set of master templates. However, waveform similarity quickly decreases with changes in the earthquake source locations or in the focal mechanisms. To account for this limitation, a smoother time series derived from the seismogram could be used for correlation. Forghani-Arani et al. (2013) use the STA/LTA trace as input for the correlation. Also seismogram envelopes are smoother functions in time than the original seismograms and are used e.g. for locating earthquakes (Withers et al. 1999; Chen et al. 2013). The smoothness also allows for down-sampling which decreases processing time in real-time analysis.

The correlation coefficient can be calculated for individual traces. Holland (2013) uses only the vertical component of seven stations while Schaff (2010) averaged the three components of one station. Alternatively, a network correlation coefficient can be computed by averaging the trace correlations, e.g. of a whole array, as introduced by Gibbons and Ringdal (2006). To improve robustness we consider both, the trace correlation coefficient with coincidence constrains as the first detection criterion, and as second detection criterion the network correlation as a matrix correlation, taking into account the amplitude decay within the network.

Cross-correlation methods are often used to improve existing catalogues, however, real-time applications are still rare. Harris and Paik (2006) worked on an optimisation of a subspace detector for real-time application. The cross-correlation detector presented here is implemented and tested in SeisComP3, which is an established tool for seismological real-time data analysis (Hanka et al. 2008).

Besides the standard STA/LTA trigger a number of different methods is used to automatically detect signals in waveform data. In pattern recognition, as used by e.g. Joswig (1990), sonograms of a set of known templates are compared to sonograms of the data, where a large range of frequencies is taken into account. Hidden Markov Models are a statistics based approach, as introduced to seismology by Ohrnberger (2001). To build a Hidden Markov Model, first a set of training data has to be available to extract the characteristic features and transition probabilities. It is advantageous for monitoring tasks where only one or a few stations are available, as described by Beyreuther et al. (2012) for volcano monitoring. Subspace detectors (Harris and Paik 2006) are another detection

method, using the approach that a signal can be modelled as the sum of weighted basis functions, i.e. template waveforms forming the representation matrix. The data are projected into the subspace spanned by the columns of the subspace representation matrix. A detection is triggered, when the ratio of the squared norm of the projected vector to the squared norm of the original data vector exceeds a given threshold value.

Besides detecting an earthquake and assigning it to a reservoir, information on the size of the event is also essential. For local networks the local magnitude scale M_L is commonly used to describe the size of an earthquake (Richter 1935). However, for induced microseismic events this definition of a local magnitude is unfavourable as the source depth is not taken into account. A number of different approaches exist to determine a magnitude focusing on local networks (Edwards et al. 2015), small events (Lee et al. 1972), or repeated seismicity (Rubinstein and Ellsworth 2010). We exploit the amplitude ratio of the detected event and the master event for magnitude calculation. Schaff and Richards (2014) showed that the application of a relative magnitude is plausible for events where the waveforms are very similar and the noise level is high.

2 Detector

The detector is based on the cross-correlation of continuously recorded data with known master events. A detection is triggered, when two detection criteria are met. Firstly, the similarity of the incoming data $\hat{f}$ with a master event $\hat{e}$ is evaluated by calculating the cross-correlation coefficient R^j of each trace j:

$$R^j = \frac{1}{\sqrt{\left[\sum_{i=1}^{L}\left(\hat{e}_i^j\right)^2\right]\left[\sum_{i=1}^{L}\left(\hat{f}_i^j\right)^2\right]}} \sum_{i=1}^{L} \hat{e}_i^j \hat{f}_i^j \qquad (1)$$

L is the length of the recent time window, i and j are the counters for time and trace number, respectively.

The first detection criterion is, that the trace correlation coefficient R^j has to exceed a defined threshold R_1 at a number of stations $\hat{M}$ and traces $\hat{N}$ larger than a minimum number of stations M_{min} and traces N_{min}, respectively.

$$R^j \geq R_1 \qquad j = 1 \ldots \hat{M} \qquad M_{min} \leq \hat{M} \leq M \qquad (2)$$

and

$$R^j \geq R_1 \qquad j = 1 \ldots \hat{N} \qquad N_{min} \leq \hat{N} \leq N. \qquad (3)$$

M and N are the total number of stations and traces, respectively. This condition implies that not all, but most data traces have to be similar to the master event traces at most stations. Thus, it accounts for local noise or data gaps as might happen due to station or data transfer problems. As different master events might be made up from different numbers of traces, not a fixed value for M_{min} and N_{min} but the fraction of the stations (M_{min}/M) and channels (N_{min}/N) of the master event is defined.

If this first detection criterion is met, secondly, the network correlation coefficient R is calculated by summing over the time window L as well as over the traces j with $R^j \geq R_1$.

$$R = \frac{1}{\sqrt{\left[\sum_{j=1}^{\hat{N}}\sum_{i=1}^{L}\left(\hat{e}_i^j\right)^2\right]\left[\sum_{j=1}^{\hat{N}}\sum_{i=1}^{L}\left(\hat{f}_i^j\right)^2\right]}} \sum_{j=1}^{\hat{N}}\sum_{i=1}^{L} \hat{e}_i^j \hat{f}_i^j. \qquad (4)$$

The network correlation coefficient is a matrix correlation not a simple average over trace correlation coefficients. Therefore, it considers the amplitude ratio at the different traces, which accounts for stations at different distances and also different site amplification factors. As second detection criterion the network correlation coefficient R has to exceed a certain threshold R_2

$$R \geq R_2. \qquad (5)$$

Figure 1 shows that the trace correlation R^j exceeds the threshold ($R_1 = R_2 = 0.7$) more often than the network correlation R, which contains information from all stations. Since the network correlation averages over all trace correlation coefficients, the influence on the network correlation coefficient of one station, e.g. the similarity between noise burst and master event, is small.

If both criteria are met, a detection is triggered. The source time is determined from the maximum of the correlation coefficient. This is searched for in a small time window after the network correlation first exceeds the threshold R_2 (panel D in Fig. 1). The source time is calculated relative to the master event's source time.

A location is not performed, but the location of the master event is adopted.

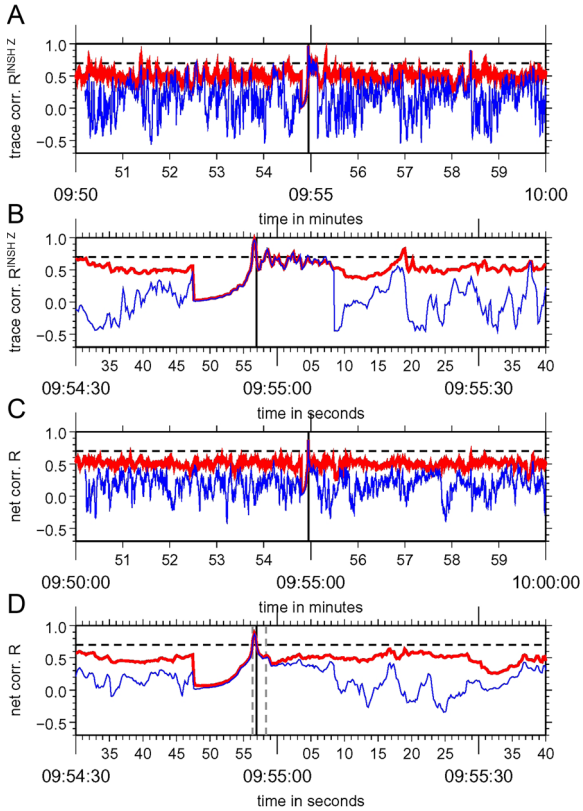

Fig. 1 The trace correlation coefficient R^{INSHZ} and the network correlation coefficient R with noise removal (*blue line*), and without noise removal (*red line*) are shown. Panels (**A**) and (**B**) (*zoom in of A*) show the trace correlation R^j for the vertical component of station INSH. In panels (**C**) and (**D**) (*zoom in of C*) the network correlation R is given. The thresholds $R_1 = R_2 = 0.7$ are given by the horizontal dashed lines. In panel D the time window to search for the maximum of the cross-correlation coefficient R after the first exceedence of the threshold is indicated by vertical dashed gray lines. In the given example this is 2 s. The origin time of the Insheim earthquake (2013-07-13, 09:54:56.8 UTC) is calculated from the maximum of the network correlation and marked by the vertical black line

In general, this detection process can be applied to the waveform itself as well as to the envelope. Full waveform template matching is extremely sensitive if the signal in the detection time window consists of one of the master events plus some additional noise. It is applicable only to strictly repetitive sources confined to regions smaller than one or two wavelengths at the dominant frequency of the repeating waveforms. Practically, the source locations and source mechanisms of the induced earthquakes vary and thus, the waveforms will not always be identical to the master event's waveform. The envelope is more stable against small changes in source location and source mechanism. This makes the envelope suitable for the purpose of monitoring a geothermal reservoir, where events might occur not only at one distinct place but scatter over the reservoir. Furthermore, the envelope is a lower frequency signal than the waveform, which allows for a resampling with coarser time steps. This results in data reduction and thus is less expensive in terms of processing performance. However, the chance of misdetections, e.g. from local tectonic events near the reservoir, slightly increases.

The causal envelope e of a trace j is calculated as

$$e_i^j = \sqrt{\frac{2}{L_m} \sum_{k=i+1-L_m}^{k=i} \left(y_k^j\right)^2}. \tag{6}$$

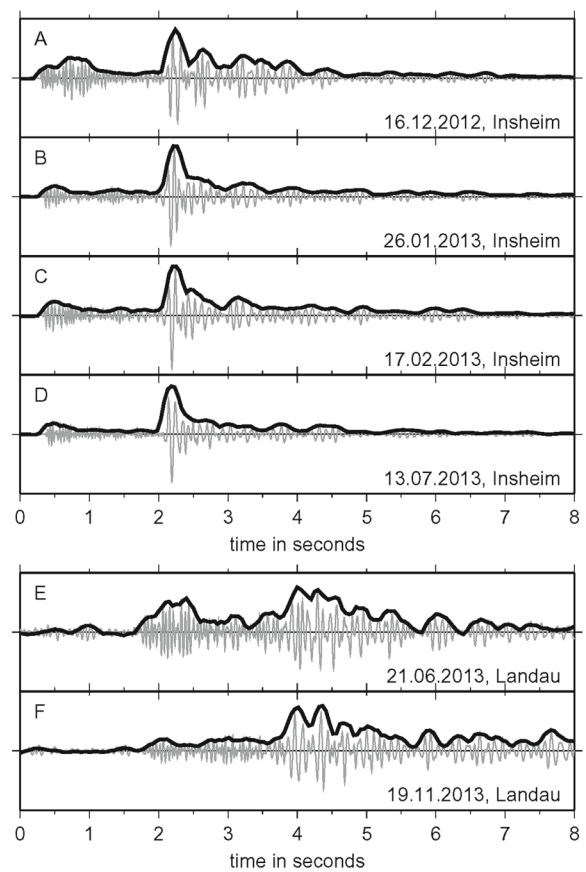

Fig. 2 Examples for events from the Insheim reservoir (A: 2012-12-16, M_L 1.4, B: 2013-01-26, M_L 1.8, C: 2013-02-17, M_L 2.0, D: 2013-07-13, M_L 1.4) and the Landau reservoir (E: 2013-06-21, M_L 1.2, F: 2013-11-19, M_L 1.5). The gray line is the seismogram and the black line the envelope. All panels show the normalized east component of station INSH

i and k are the time step counters and y_k^j denotes the bandpass filtered seismogram of which the envelope is calculated. Averaging is carried out over L_m data points to smooth the waveform in time. This is done for the incoming data as well as for the master events. Figure 2 gives an example of waveform data and their envelopes for events from the two neighbouring geothermal reservoirs in Insheim and Landau.

The standard deviation of the local noise results in a positive offset of the envelope (Fig. 3). As a consequence, the correlation gives a comparatively high correlation coefficient, although only noise is recorded (Fig. 1). We solve this issue by subtracting the noise from the data envelope as well as from the master event envelope. The noise e_{noise}^j at a trace j is defined as the average over a small time window preceding the seismic signal

$$e_{noise}^j = \frac{1}{L_n} \sum_{i=1}^{L_n} e_i^j . \tag{7}$$

i is the time step counter and L_n is the length of the noise time window. This defines the noise corrected envelope as $\hat{e}_i^j = e_i^j - e_{noise}^j$. Consequently, we use the noise corrected envelope of the master event $\hat{f}_i^j$ and the noise corrected envelope of the incoming data $\hat{e}_i^j$ for cross-correlation ((1) and (4)). Figure 3 is showing the process of the noise removal at the envelope. At a certain time during the processing the noise time window might contain a local noise burst or a seismic signal simulating a high noise level. Thus, a second noise time window is defined, and the smaller noise value of both windows will be used for subtraction. The time between the two noise windows should be greater than the signal length L, so that a signal never contains both noise time windows during one processing step.

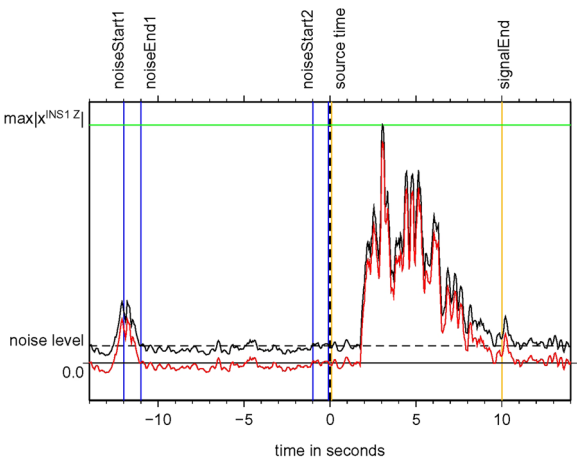

Fig. 3 Envelope of vertical component of station INS1 (*black line*) for the Insheim event of 2013-07-13, 09:54 UTC. The preceding noise causes a small positive offset in the envelope. This average noise level is estimated in the two noise time windows [noiseStart1 noiseEnd1] and [noiseStart2 noiseEnd2] marked by vertical blue lines. The envelope is corrected by subtracting the noise level, as shown by the red line. Signal length L is defined as a time window from signalStart to signalEnd (*vertical orange lines*). The event's source time is marked by the dashed black line. The maximum of the absolute value of the envelope is used to compute the magnitude (*green line*)

Several master events can be included in the detection process. These can be master events from different reservoirs, e.g. Insheim and Landau, or a number of master events for one distinct location. In the latter case, the detector allows to group master events e.g. to create a group "Insheim" with a set of master events from different parts of the Insheim reservoir. If the detection criteria are met for more than one master event of a group, the master event with the highest network correlation defines source time, location, and magnitude of the new detection.

To detect even smallest events when monitoring a clear target, e.g. one geothermal reservoir, the thresholds will be set considerably low. Thus, events from a nearby region, e.g. local tectonic events, might cause misdetections. The detector can be trained to know these events as negative master events, so that if the recent data are similar to this negative master events, a detection is triggered but not sent out.

For a most effectively working online detector the handling of real-time data is an essential part. Therefore, the detector is implemented as a SeisComP3 module, taking advantage of this system. One point in dealing with real-time data is a possible delay in data transmission or outages of stations. A timeout is defined for how long the detector will wait for missing data to arrive. If they are not available during this time period, the processing skips these data and moves on setting $R^j = 0$ for this trace. Besides the real-time mode it is also possible to run the detector on archived data as an offline playback, e.g. to search for events similar to a new master event or for adjusting the processing and detection parameters.

3 Magnitude estimation

After detecting the earthquake, real-time magnitude estimation is important for seismic response plans. Microseismic events are weak so that their signal quickly decays below the local noise level, and the amplitude of the seismic signal cannot be measured at greater distances. At a local network with event depth in about the same order of magnitude as the network radius, the event depth contributes significantly to the amplitude decay as a function of hypocentral distance. For calculating M_L, however, the source depth is not taken into account, as it was developed for tectonic events recorded at a certain distance. Also, the Wood-Anderson instrument, that Richter (1935) used to determine M_L, is not used anymore in modern seismology. Digital simulation is possible but the frequency band of the Wood-Anderson instrument is not suitable for the high frequency content of the microseismic events. Thus, an approach different from the original M_L definition is needed. We compute a relative magnitude from the ratio of the maximum amplitude value of a known event and a newly detected event. The master event has to be strong enough to be recorded at distant stations, so that the local magnitude $M_{L,x}$ can be determined. For each trace j, that meets the first detection criterion (3), a trace magnitude $M^j_{L,y}$ is calculated from the amplitude ratio between master event x and event y using

$$M^j_{L,y} = M_{L,x} + log_{10}\left(\frac{max_i|y^j_i|}{max_i|x^j_i|}\right). \tag{8}$$

$max_i|x^j_i|$ and $max_i|y^j_i|$ denote the maximum amplitude of the data trace and the corresponding master event's trace, respectively. If all three components of one station meet detection criterion 1, we estimate three trace magnitudes for this station. When using the envelope for correlation, $max_i|x^j_i|$ and $max_i|y^j_i|$ are the maxima of the envelopes. The network magnitude $M_{L,y}$ is determined by averaging over all $\hat{N}$ traces that meet the detection criterion in (3):

$$M_{L,y} = \frac{1}{\hat{N}}\sum_{j=1}^{\hat{N}} M^j_{L,y}. \tag{9}$$

This relative magnitude differs from the local magnitude as an arbitrary bandpass filter is used instead of a Wood-Anderson simulation filter. As a consequence the relative magnitude will only resemble M_L for a reasonable bandpass filter and for magnitudes in the magnitude range of the master event.

4 Application to induced seismicity at the Insheim and Landau geothermal reservoirs in the upper rhine graben

To test the cross-correlation detector's performance, it is applied to the monitoring of induced seismicity at the two neighbouring geothermal reservoirs in Insheim and Landau in the German part of the Upper Rhine Graben (URG). Firstly, an offline playback is run for a short period of data with the focus on the Insheim reservoir. Secondly, the detector is deployed in real-time to the two reservoirs in Insheim and Landau for one year. The detections from the reservoirs as well as from the nearby quarry Waldhambach are analysed.

4.1 Geological setting, geothermal plants and seismic network

The Upper Rhine Graben (URG) is part of the NNE-striking European Cenozoic rift system, which extends from the western Mediterranean to the North Sea (Illies 1972; Ziegler 1992). Despite of being among the seismically most active regions in Germany, the seismic risk at the URG is small to moderate relative to the European scale (Leydecker 2011; Grünthal and Wahlström 2012). The most damaging earthquake occurred at the southern end of the URG near Basel in 1356 with a moment magnitude between 6.7 and 7.1 and a maximum intensity of IX near the epicenter (Fäh et al. 2009).

The URG is the region with the highest geothermal gradient in Germany, e.g. more than 150 °C are reached at depths of 2500 m in the northern part of the graben (Agemar et al. 2014). This makes the region one of the focus areas for geothermal energy production in Germany. Widely known are the projects in Soultz-sous-Forêts (France) (Evans et al. 2005) and Basel (Switzerland) (Häring et al. 2008). The first geothermal power plant in the German part of the URG became operational in Landau in 2007. This plant has a doublet configuration with two boreholes drilled down to 3300 m and 3340 m, respectively, with

a horizontal distance of about 1500 m at depth. The plant was built to generate 2.9 MW of electric and 24 MW of thermal energy (Baumgärtner et al. 2013). The maximum flow rate reaches 70 l/s, and the production temperature is about 155 °C to 160 °C (Hettkamp et al. 2013). Since March 2014 the production has been stopped because of significant surface uplift around the power plant. The uplift is not linked to the seismically active reservoir as it is caused by near surface leakage problems (Heimlich et al. 2015). About 4 km south of Landau, a second power plant commissioned in Insheim in November 2012. It is designed to generate a total power of 4.8 MW electric and optionally 38 MW of thermal energy with a production rate up to 80 l/s. Temperatures of more than 165 °C are measured at 3800 m (Baumgärtner and Lerch 2013; Baumgärtner et al. 2013). Both power plants are Enhanced Geothermal Systems with a multi-horizon approach, which aims at the production of thermal fluid from several horizons in the transition zone from the Mesozoic sediments to the crystalline basement (Baumgärtner and Lerch 2013). The plants are situated in the region of the Landau block system at the western central URG. The top of the crystalline basement is about 2400 m beneath Landau and at 3000 m to 3500 m beneath Insheim (GeORG Project Team 2013).

Significant tectonic seismicity in the study area is only known near Kandel, about 10 km south of Insheim, with a maximum intensity of V in 1880 and VI in 1903, respectively (Barth 2011). Since 2006 three events with $M_L \geq 2$ from Landau have been recorded and eight such events from Insheim (Landesamt für Geologie und Bergbau Rheinland-Pfalz 2015). Altogether more than 2200 induced microevents have been detected since 2006. Most of these events were not perceived. Only a few have been felt by the local population (Groos et al. 2013). After the first occurrence of two felt induced earthquakes near Landau with local magnitudes of 2.7 and 2.4 in 2009 (Bönnemann et al. 2010), the production rate of the power plant was reduced to 55 l/s

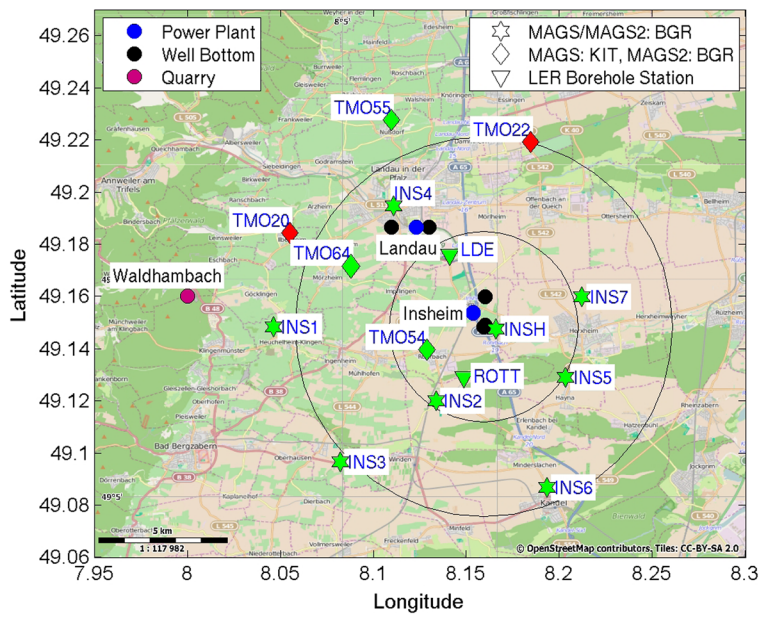

Fig. 4 Seismic monitoring network around the geothermal power plants in Insheim and Landau (*blue dots*) during the MAGS project. The black dots mark the well bottoms with the injection wells being the eastern well for Landau and the southern well for Insheim, respectively. The quarry in Waldhambach is marked in purple. Stations operated by BGR are marked with stars and those operated by KIT during MAGS with diamonds. The filling displays, if the data were available in real-time via online data transfer (*green*) or if the data were stored at the station (*red*) during MAGS. For MAGS2 the KIT's stations were changed to BGR online stations. The network is centred at the Insheim injection well. Two circles with 4 km and 8 km radius, respectively, mark the single and the double reservoir depth. The two borehole stations ROTT (depth 305 m) and LDE (depth 150 m) (*triangles*) are available from the Geological Survey and Mining Authority of Rhineland-Palatinate (LER) for MAGS2. TMO64 (depth 70 m) is an additional borehole station

(Hettkamp et al. 2013). Additionally, as a consequence the seismic monitoring was improved. On behalf of the power plant's owner the local seismological network was complemented by an immission network to record the peak ground velocities (PGV) of seismic events according to German DIN4150 standards (Deutsches Institut für Normung e.V. 2015). Additionally, a temporary network of seismological stations was installed within the framework of the research project "MAGS - Microseismic Activity of Geothermal Systems". The network (see Fig. 4) is set up within a radius of 8 km corresponding to the double reservoir depth as recommended in Baisch et al. (2012). To account for the high frequency content of small events, the sampling rate is set to 200 Hz at all stations.

Comprehensive analyses of the seismicity for the years 2006 to 2013 were performed by Groos and Ritter (2014). Since October 2013 the seismicity is analysed at BGR and the local seismological survey of the Geological Survey and Mining Authority of Rhineland-Palatinate (LER). In the following sections, we describe the application of the automatic detector and compare the results to the manually revised catalogues.

4.2 Offline test

To validate the performance of the new envelope cross-correlation detector continuous seismological data from the waveform archive are automatically processed. In this offline playback we first focus on the Insheim reservoir. The automatic detection list is compared to the manual one, thoroughly processed by the Karlsruhe Institute of Technology (KIT), as reference (Groos and Ritter 2014). This KIT catalogue was constructed from waveform cross-correlation of known events with continuous data of one component using normalized amplitudes. Detections were iteratively included as new master events. From the resulting list, detections were selected for manual inspection (Grund et al. 2016; Plenkers et al. 2013). From stronger events, relations between local magnitude M^{LE} (Stange 2006) and peak ground velocity (PGV, in mm/s) ($M^{LE} = a^j \cdot \log_{10}\left(\mathrm{PGV}^j\right) + b^j$) are derived and applied to estimate magnitudes M^{KIT} even for small events. The resulting manually revised catalogue lists 141 events with magnitudes from -0.6 to 2.0 for Insheim for the time period 2012-11 to 2013-02. The same four months are processed using the envelope cross-correlation detector with two master events from the Insheim reservoir (see Table 1). Since a reliable location and a local magnitude are needed, we chose events with the largest magnitudes. We constructed the two master events of data from those seven stations that showed the most distinct signals. If not only the seven stations with the best signal to noise ratio are included in the master event, but also stations at larger distances, the detector's sensitivity to small events decreases. The first detection criterion defines the minimum number of stations and of channels at which the trace correlation coefficient R^j has to exceed the detection threshold R_1. $M_{min}/M = 0.7 \mathrel{\widehat{=}} 70\ \%$ for the minimum required number of stations and $N_{min}/N = 0.6 \mathrel{\widehat{=}} 60\ \%$ for the number of channels give a good compromise between detector sensitivity and number of misdetections for the monitoring setup analysed here. Using master events containing seven stations with three components each, this means that at more than five stations and 13 out of 21 channels the trace correlation R^j has to exceed R_1 to meet the first detection criterion. The stations of the master event show a good azimuthal coverage which is also the case for all detections, since at least five stations are required for a detection. Both detection thresholds (R_1 for the trace correlation coefficient and R_2 for the network correlation coefficient) are set to 0.7. The length of the noise time windows is one second, and the signal time window is 10 s. As our network is situated in urban areas, often electronic noise

Table 1 Parameters of the two Insheim master events used for the offline test according to Seismological Service of Southwestern Germany (LE) (Landesamt für Geologie und Bergbau Rheinland-Pfalz 2015)

	Insheim Master 1	Insheim Master 2
Source	2013-01-26	2013-02-17
time	19:48:27.710 (UTC)	20:07:15.750 (UTC)
Location	49.159N ± 0.6 km	49.161N ± 0.6 km
	8.153E ± 0.8km	8.152E ± 0.7km
Depth	5 ± 2 km	4 ± 2 km
M_L	1.8	2.0
Stations	INS1, INS2, INS5, INS7, INSH, TMO54, TMO64	INS1, INS2, INS5, INS7, INSH, TMO54, TMO64

with a frequency of 50 Hz is present in the data. Also the small events typically have a frequency of about 20 Hz. Therefore, data and master events are bandpass filtered at 10 - 40 Hz.

The automatically generated catalogue consists of 131 events with magnitudes between -0.7 and 2.0. The magnitude frequency distribution comparing both catalogues is given in Fig. 5 showing a similar distribution with most events between $M = -0.2$ and $M = 0.5$.

The magnitude of completeness M_c is a statistical value, describing down to which magnitude all events are listed in a certain catalogue. We use the maximum curvature of the cumulative magnitude frequency distribution to approximate M_c. Due to the limited number of events, this will give only a conservative estimation of M_c (Woessner and Wiemer 2005). For the automatic catalogue it is $M_c^{MAGS} = -0.1$ and $M_c^{KIT} = 0.1$ for the manually processed reference catalogue (Fig. 5).

Panels C and D in Fig. 5 show the events listed in either only the automatic catalogue (panel C), or only in the reference catalogue (panel D). All events with magnitudes larger than 0.5 are listed in both catalogues. 29 events are listed only in the automatic catalogue. To validate the automatic catalogue, these events are inspected manually. Only one event is a false detection due to local noise bursts at some neighbouring stations and one is probably a small local tectonic event. This results in less than 2 % misdetections in the automatic catalogue. The remaining 27 Insheim detections are events that the KIT catalogue, derived from waveform cross-correlation, missed, but were found by the envelope cross-correlation detector. The largest one of these events has a magnitude of 0.1. The automatic envelope detector missed 26 events of the KIT catalogue with a local magnitude larger than −0.1. Visual inspection shows that these events are identifiable only at very few stations and thus do not fulfil the first detection criterion. Also,

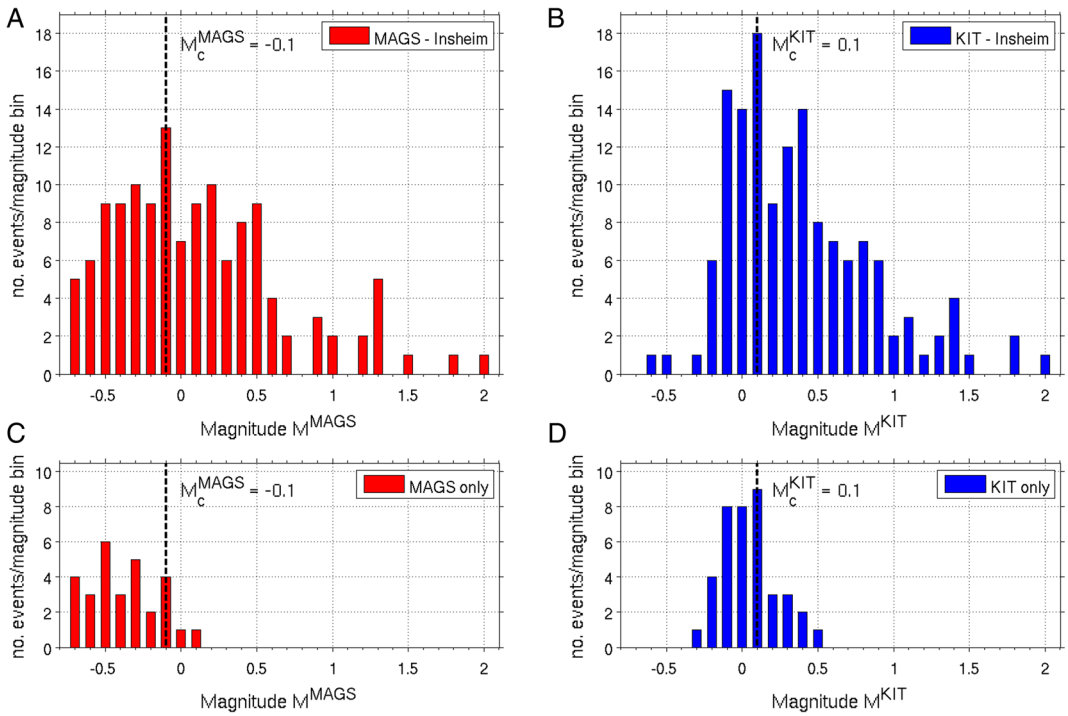

Fig. 5 Magnitude frequency distribution of Insheim events listed in the automatically generated catalogue (envelope cross-correlation detector, red bars in panels A and C) and the manually verified KIT catalogue (waveform cross-correlation detector, blue bars in panels B and D) for November 2012 until February 2013. The maximum of the curvature of the cumulative distribution gives the magnitude of completeness for the respective catalogue: M_c^{MAGS} = - 0.1 and M_c^{KIT} = 0.1 (*black dashed lines*). While panels A and B show the full catalogues, panels C and D show the histograms of events listed in only one of the catalogues, i.e. only in the automatic (panel C) or only in the reference catalogue (panel D)

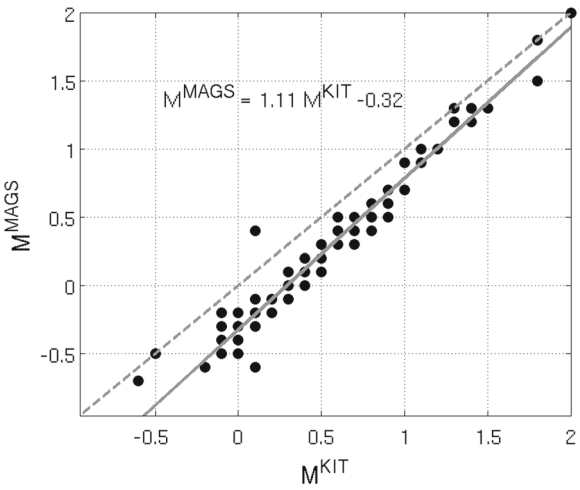

Fig. 6 Comparison of the magnitudes estimated from the amplitude ratios in the automatic catalogue M^{MAGS} and the local magnitude in the reference catalogue M^{KIT}. Events listed in both catalogues are plotted as black dots. An orthogonal distance regression (*solid gray line*) is applied to the data. The dashed gray line indicates the ideal relation where M^{MAGS} equals M^{KIT}

the KIT catalogue was constructed from a very sensitively tuned waveform cross-correlation with manual inspections.

Figure 6 compares the magnitudes of the events listed in both catalogues. The magnitudes of the automatic catalogue are determined by the detector from the amplitude ratio as described by (9), while the manual catalogue contains local magnitudes M_L according to Groos and Ritter (2014). The orthogonal distance regression results in

$$M^{MAGS} = 1.11\, M^{KIT} - 0.32. \quad (10)$$

The slope of the regression line is slightly larger than one. This means, that the magnitudes calculated from the amplitude ratios underestimate the smaller magnitudes, while for larger magnitude values they fit with the local magnitudes of Groos and Ritter (2014). The mean magnitude difference is 0.23 and the standard deviation is 0.13. Correcting $M_c^{MAGS} = -0.1$ according to (10) would give a magnitude of completeness of 0.2 for the automatic catalogue.

4.3 Online test

A real-time detection system was installed in October 2013. As the data of the online stations usually arrive at the data centre within less than two minutes, the time-out of the detector to wait for missing data is set to 5 min. Consequently, the processing might be delayed by a maximum of five minutes from real-time. Noise as well as signal time window length are used as in the offline playback.

As the seismic network changed in October 2013 (end of MAGS, beginning of follow-up project MAGS2), new master events are defined for the online test. Additional to Insheim, we include templates for the Landau geothermal reservoir and the neighbouring quarry in Waldhambach (see Table 2). As we use the envelope of the seismogramms, the implementation of one master event per reservoir has proven sufficient. This is in contrast to waveform cross-correlation for the same reservoirs (Grund et al. 2016; Groos and Ritter 2014) where several templates for each reservoir were used. To test, if also the same detection thresholds ($M_{min}/M = 70\,\%$, $N_{min}/N = 60\,\%$, $R_1 = 0.7$, $R_2 = 0.7$) are equally suitable when monitoring not

Table 2 Parameters of the Insheim, Landau and Waldhambach master events used for the real-time test according to the local seismological survey of the Geological Survey and Mining Authority of Rhineland-Palatinate (Landau/Insheim: Landesamt für Geologie und Bergbau Rheinland-Pfalz (2015), Waldhambach: Brüstle and Schmidt pers. comm., 2015)

	Insheim	Landau	Waldhambach
Sourcetime	2013-10-02	2013-11-19	2014-05-06
	01:13:26:80 (UTC)	11:07:43.00 (UTC)	09:50:49.00 (UTC)
Location	49.162N ± 0.7 km	49.190N ± 1 km	49.159N
	8.152E ± 0.7 km	8.110E ± 1 km	8.004E
Depth	4 ± 1 km	3 ± 2 km	0 km
M_L	2.1	1.5	1.5
Stations	INS1, INS2, INS7, INSH, TMO54, TMO64, LDE	INS1, INS4, TMO20, TMO54, TMO55, TMO64, LDE	INS1, INS3, TMO20, TMO54, TMO55, TMO64, LDE

Table 3 Overview of correct detections, misdetections and missed events for one day (2014-06-08) using different detection thresholds

M_{min}/M	correct detections	misdetections	missed events	N_{min}/N	correct detections	misdetections	missed events
50 %	14	2	3	40 %	15[1]	3	3
60 %	14	2	3	50 %	14	2	3
70 %	14	2	3	60 %	14	2	3
80 %	11	2	6	70 %	12	2	5
90 %	11	2	6	80 %	10	0	7
R_1	correct detections	misdetection	missed events	R_2	correct detections	misdetection	missed events
0.5	14	0	3	0.5	15	2	2
0.6	14	1	3	0.6	14	2	3
0.7	14	2	3	0.7	14	2	3
0.8	12	0	5	0.8	14	1	3
0.9	3	0	14	0.9	7	0	10

[1]One new event is detected, that is not listed in the LER catalogue

At each block one of the detection thresholds is varied from $M_{min}/M = 70$ %, $N_{min}/N = 60$ %, $R_1 = 0.7$, $R_2 = 0.7$ as given in the respective first column

only Insheim, but also including the Landau reservoir and a nearby quarry (see Table 2), we vary the values and combinations of M_{min}/M, N_{min}/N, R_1 and R_2. Table 3 gives an overview of correct detections, misdetections and events missed for one day (2014-06-08) compared to the detailed LER catalogue (description see below, Fig. 9). It shows that generally, when the detection thresholds are higher, the number of missed events increases, and the number of correct detections decreases. A low threshold for the trace correlation coefficient gives less misdetections because including traces with low similarity to the master event into the network correlation, results in a lower network correlation coefficient. No new events are detected, except when setting N_{min}/N to 40 %, which at the same time causes one misdetection from noise. All other misdetections are caused by one tectonic event, that was wrongly detected as quarry blast and in some

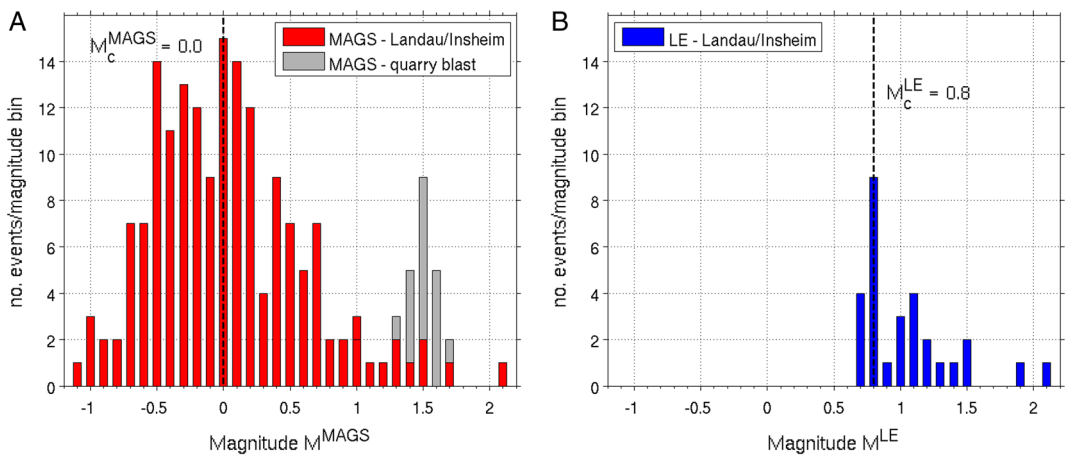

Fig. 7 Magnitude frequency distributions for the events in Insheim and Landau for the time period October 2013 to September 2014 as listed in the automatically generated catalogue (*panel A, red bars*) and in the public LE catalogue as reference (*panel B, blue bars*). A conservative estimation of the magnitude of completeness is given from the maximum curvature of the cumulative distribution as $M_c^{MAGS} = 0.0$ and $M_c^{LE} = 0.8$. The quarry blasts listed in the automatic catalogue (*gray bars*) show magnitudes around 1.5. The local tectonic events that are misdetected as Insheim or Waldhambach events (see Table 4) are not considered here

cases also the S-Phase was misdetected as Insheim event. Altogether, the setting used for the offline test with only Insheim master events, is also applicable to monitoring three different targets (Table 2).

The automatic catalogue for one year of monitoring (2013-10-01 to 2014-09-30) is compared to the public event bulletin from the routine analysis of the Seismological Service of Southwestern Germany (LE) (Landesamt für Geologie und Bergbau Rheinland-Pfalz 2015). The catalogue is constructed by running an adjusted Baer-Kradolfer picker (Baer and Kradolfer 1987) on a 3 min time window and applying temporal and spacial coincidence conditions on the resulting picks. In case of a detection, the waveform data of further stations are requested, optimising the data set for local, regional or teleseismic processing. The picker is run again, defining the final phase arrivals that are than used for location. Depending on the quality of the detection, the results are rejected, manually revised or automatically published at the online event bulletin (pers. comm. S. Stange, 2016).

Figure 7 shows the Insheim and Landau detections from the automatic catalogue as red bars in panel A and in comparison the public LE event bulletin as blue bars in panel B. Local tectonic events that are misdetected as Insheim or Waldhambach events (see Table 4) are not considered here. A conservative measure for the magnitude of completeness is estimated from the maximum curvature of the cumulative magnitude frequency distribution. This results in $M_c^{MAGS} = 0.0$ for the automatic catalogue and in M_c^{LE} =0.8 for the LE bulletin. The quarry blasts listed in the automatic catalogue (gray bars in Fig. 7) show magnitudes around 1.5 and form a different magnitude frequency distribution. One M_L 1.9 event of the LE catalogue seems to be missing in the MAGS catalogue, however, the magnitude from the amplitude ratio for this event is smaller (M^{MAGS} 1.7) and, consequently, it is assigned to a different magnitude bin in the histogram. Thus, all events of the LE catalogue are included in the automatic catalogue.

The manual catalogue comprises local magnitudes M_L according to Stange (2006). Figure 9 compares the magnitudes for the events that are listed in both catalogues. An orthogonal distance regression is fit to the data according to

$$M^{MAGS} = 1.19\, M^{LE} - 0.33. \tag{11}$$

Events with a magnitude $M^{LE} \leq 1.1$ are assigned a smaller weight of 0.1 for the orthogonal distance regression as the magnitudes M^{LE} scatter for smaller events. The slope of the linear regression is slightly higher than one, meaning that the smaller magnitudes are underestimated by the detector, while for larger magnitude values the magnitudes from amplitude ratio fit with the local magnitudes.

The automatic detection is send out via email with the SeisComP3 xml-file of the event including source and detection parameters attached. It serves as a starting point for the manual determination of phase arrivals and precise location of the event at the local seismological survey of the Geological Survey and Mining Authority of Rhineland-Palatinate (LER) within the research project MAGS2. This manual LER catalogue is used for a detailed comparison. It also includes the detections reported to the LER by the companies conducting the seismic monitoring on behalf of the plants' owners (Insheim: BESTEC for Nature GmbH, Landau: DMT since spring 2014, formerly BESTEC). They maintain additional stations and different detection algorithms, which makes the LER catalogue a comprehensive reference list.

Table 4 Evaluation of the automatic catalogue for the real-time test

	Insheim	Landau	Waldhambach
detections	142	35	35
correctly associated	137 (96 %)	35 (100 %)	27 (77 %)
misdetections - tectonic events	5 (4 %)	0	8 (23 %)
missed events (manual LER catalogue)	32	15	0

The detections are compared to the manual catalogue of the local seismological survey that was compiled within the framework of the research project "'MAGS2" at the Geological Survey and Mining Authority of Rhineland-Palatinate (LER). It includes the automatic detections and also the reported detections from the monitoring companies

The automatic catalogue consists of 212 events out if which 172 induced events are correctly associated to the geothermal sites in Insheim and Landau (Table 4). 35 detections are assigned to the quarry in Waldhambach. Figure 8 shows a comparison of the magnitude frequency distribution for the geothermal reservoirs in Insheim (panel A), Landau (panel B) and the quarry in Waldhambach (panel C). Altogether, for the analysed time period the manual LER catalogue contains 87 events that are missed by the automatic detector (blue bars). 47 of these 87 detections missed by the automatic detector are induced events, and the remaining 40 detections are not locatable because the signals are too weak. To ensure comparability, the magnitudes of these events are deduced from manually applying an offline playback on the respective source times of the events missed by the real-time detector. It showed that all, but one of these events can be detected if the detection criteria are tuned down at the expenses of an increased misdetection rate.

For Insheim, the real-time detector lists 137 correctly assigns events (Table 4; red bars in Fig. 8a) and 32 missed events (blue bars) at a magnitude range of $M^{MAGS} = -0.9$ to 0.3. Also, five tectonic events outside of the geothermal reservoir are wrongly assigned as Insheim events (green bars). The magnitude of completeness for the Landau events can

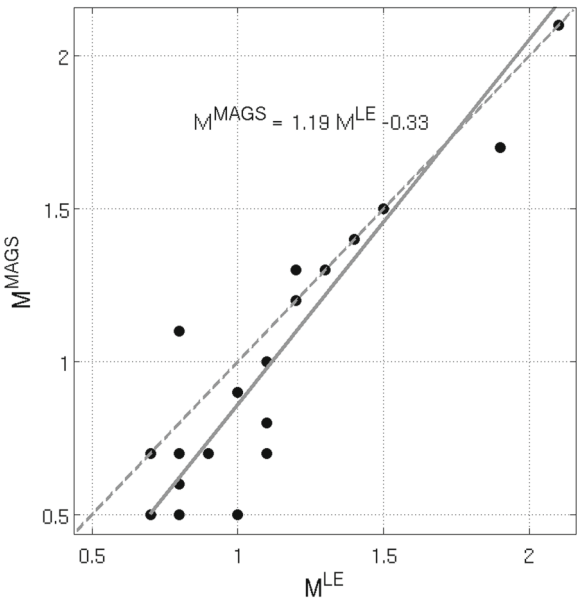

Fig. 8 Magnitudes calculated from amplitude ratio by the detector (M^{MAGS}) versus the local magnitude from the reference LE online bulletin for events listed in both catalogues (*black dots*). An orthogonal distance regression (*solid gray line*) is fitted to the data, assigning a smaller weight of 0.1 to events with $M^{LE} \leq 1.1$ as they scatter. The dashed gray line indicates the ideal relation $M^{MAGS} = M^{LE}$

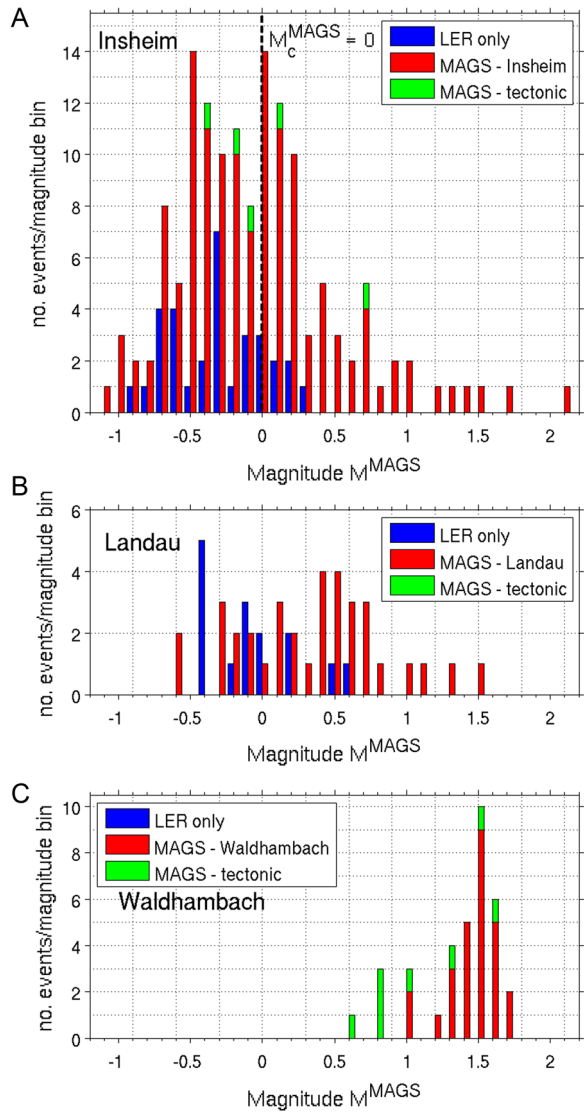

Fig. 9 Comparison of the magnitude frequency distribution for the automatic MAGS catalogue from real-time envelope cross-correlation and the manually revised LER catalogue for the geothermal reservoirs in Insheim (**A**) and Landau (**B**) as well as the quarry in Waldhambach (**C**). Red bars show the automatically correctly assigned events, green bars the local tectonic events misdetected as induced events. Blue bars are the events, listed in the LER catalogue only, missed by the detector. The magnitudes of these events were derived by manually applying an offline playback with lower detection criteria on the respective times. The dashed black line marks the magnitude of completeness of the combined automatic catalogue

not be calculated due to the small number of events. Figure 9, panel B indicates that it might be slightly larger than for the Insheim reservoir. The Landau detections are all correctly associated. However, the real-time detector missed 15 events that are listed in the LER catalogue (blue bars in Fig. 8, panel B). They are at a magnitude range of $M^{MAGS} = -0.3$ to 0.6 whereof four events have $M^{MAGS} > M_c^{MAGS} = 0.0$.

Panel C of Fig. 8 shows, that the manual catalogue lists no further events from the quarry in Waldhambach, but wrongly assigned eight local tectonic events as quarry blasts. A possible reason is, that the quarry is outside the network and thus the azimuthal coverage is not sufficient (Fig. 4).

5 Discussion and conclusion

Microseismic real-time monitoring demands a detector that reliably reports small events, ideally without misdetections even if the seismic network is situated in a noisy environment. Standard STA/LTA triggers tend to fail at this task. Correlation methods more reliably detect repeated seismic events, but have rarely been applied in real-time. We implemented a real-time envelope cross-correlation detector in SeisComP3 and applied it to the monitoring of the neighbouring geothermal reservoirs in Insheim and Landau and a nearby quarry in the Upper Rhine Graben.

Two time periods were analysed in detail. For the four months of 2012-11 to 2013-02, an automatic catalogue with 131 events was created by offline processing for Insheim. Maximum curvature gives a magnitude of completeness of $M_c^{MAGS} = -0.1$. The comparison to a manually verified catalogue, derived from waveform cross-correlation, showed that both catalogues have a similar magnitude of completeness and all larger events are listed in both catalogues. The automatic envelope cross-correlation catalogue contains 27 new events and 2 % misdetections.

The second time period is 2013-10-01 to 2014-09-30. Here, not only Insheim, but also master events from the neighbouring geothermal reservoir in Landau and the quarry in Waldhambach are included for real-time processing. The master event used for the blasts in Waldhambach caused several misdetections, probably because the quarry is outside the network. The resulting automatic catalogue lists 177 events from the geothermal reservoirs with 96 % of the Insheim events and all of the Landau events assigned correctly to the respective source. The distinction between the two neighbouring reservoirs and the quarry worked reliably. The real-time catalogue includes all events listed in the public event bulletin of the Seismological Service of Southwestern Germany for the analysed time period and region. For a more extensive analysis, the automatic catalogue is compared to the detailed LER catalogue, which contains 47 additional locatable micro-earthquakes detected by the monitoring company using more stations. These events can be found by the envelope cross-correlation detector, only if the detection criteria are lowered. However, this would increase the rate of misdetections. The automatic catalogue lists five local tectonic events that are wrongly identified as Insheim events. No misdetections from noise bursts are listed.

According to Groos et al. (2013) the seismic events in Landau with $M_L > 1.3$ are perceptible. DIN4150 (Deutsches Institut für Normung e.V. 2015) gives a threshold for peak ground velocity of 3 mm/s up to which minor damages at very sensitive buildings can no longer be ruled out. Groos et al. (2013) showed, that this threshold is not exceeded for events with $M_L < 2$. Thus, with a magnitude of completeness of $M_c^{MAGS} = 0.0$ the automatic catalogue gives a good basis for response plans, that estimate the expected number of larger events using the Gutenberg-Richter relation. For reservoir characterisation, however, the setup might be chosen different, e.g. a set of master events from different parts of the reservoir could be used and the threshold would be considerably lower.

The magnitudes estimated from the amplitude ratio reproduce the local magnitudes close to the magnitude of the master event, but tend to have a small offset for smaller earthquakes. Using a master event with a medium magnitude of the expected range of magnitudes or including a set of master events with different magnitudes might solve this problem. Given the case that no reference magnitude is available, still any plausible value could be selected as the master event's magnitude to allow relative magnitude calculation as a basis for b-value estimation. A method to calculate relative magnitudes without a reference magnitude is discussed by Cleveland and Ammon (2015).

Acknowledgments This study was performed in the framework of the joint projects MAGS and MAGS2. The projects were funded by the German Federal Ministry for Economic

Affairs and Energy (BMWi) and supervised by Project Management Jülich (PtJ) (BMWi grand numbers 0325191A-F and 0325662A-G, respectively). We thank Joachim Ritter, Jens Zeiss and Jörn Gross for providing the thoroughly processed catalogue and the seismic data of the KIT online stations. Many thanks to BESTEC for nature GmbH, Pfalzwerke GmbH and geo x GmbH for the open and fruitful cooperation. Also the technical support by the BGR colleagues Mark Hanneken and Erwin Hinz for maintaining the BGR mobile stations and the help by Mathias Hoffmann regarding SeisComP3 issues are gratefully acknowledged. We also want to thank the two anonymous reviewers for their detailed reviews that helped to significantly improve the manuscript.

References

Agemar T, Weber J, Schulz R (2014) Deep geothermal energy production in Germany. Energies - Special Issue Geothermal Energy - Delivering on the Global Potential, vol 7. doi:10.3390/en7074397

Baer M, Kradolfer U (1987) An automatic phase picker for local and teleseismic events. Bull Seismol Soc Am 77(4):1437–1445

Baisch S, Fritschen R, Gross JC, Kraft T, Plenefisch T, Plenkers K, Ritter JR, Wassermann J (2012) Empfehlungen zur Überwachung induzierter Seismizität - Positionspapier des FKPE. Mitteilungen der Deutschen Geophysikalischen Gesellschaft:17–31. in German

Barth A (2011) Die Erdbeben in Kandel/Südpfalz von 1880 und 1903. Bautechnik 88(12):860–865. in German

Baumgärtner J, Lerch C (2013) Geothermal 2.0: The Insheim geothermal power plant, the second generation of geothermal power plants in the Upper Rhine Graben. In: BESTEC GmbH, Review, Third European Geothermal, Papers and Abstracts, pp. 910

Baumgärtner J, Hettkamp T, Teza D, Kölbel T, Merger H, Schlagermann P, Lerch C (2013) Betriebserfahrung mit den Geothermiekraftwerken Landau, Insheim und Bruchsal. bbr - Leitunsgbau, Brunnenbau. Geothermie 5:48–58. in German

Beyreuther M, Hammer C, Wassermann J, Ohrnberger M, Megies T (2012) Constructing a Hidden Markov Model based earthquake detector: application to induced seismicity. Geophys J Int 189(1):602–610. doi:10.1111/j.1365-246X.2012.05361.x

Bobrov D, Kitov I, Zerbo L (2014) Perspectives of cross-correlation in seismic monitoring at the International Data Centre. Pure Appl Geophys 171(3-5):439–468. doi:10.1007/s00024-012-0626-x

Bommer JJ, Oates S, Cepeda JM, Lindholm C, Bird J, Torres R, Marroquín G, Rivas J (2006) Control of hazard due to seismicity induced by a hot fractured rock geothermal project. Eng Geol 83(4):287–306. doi:10.1016/j.enggeo.2005.11.002

Bönnemann C, Schmidt B, Ritter JR, Gestermann N, Plenefisch T, Wegler U (2010) Das seismische Ereignis bei Landau vom 15. August 2009 - Abschlussbericht der Expertengruppe Seismisches Risiko bei hydrothermaler Geothermie. Tech. rep., BGR Hannover, in German

Chen CH, Chao WA, Wu YM, Zhao L, Chen YG, Ho WY, Lin TL, Kuo KH, Chang JM (2013) A seismological study of landquakes using a real-time broad-band seismic network. Geophys J Int 194(2):885–898. doi:10.1093/gji/ggt121

Cleveland KM, Ammon CJ (2015) Precise relative earthquake magnitudes from cross correlation. Bull Seismol Soc Am 105(3):1792–1796. doi:10.1785/0120140329

Deutsches Institut für Normung e.V. (2015) DIN 4150-3:2015-10: Messung von Schwingungsimmissionen - Teil 3: Einwirkungen auf bauliche Anlagen. In German

Dodge DA, Walter WR (2015) Initial global seismic cross-correlation results: Implications for empirical signal detectors. Bull Seismol Soc Am 105(1). doi:10.1785/0120140166

Edwards B, Kraft T, Cauzzi C, Kästli P, Wiemer S (2015) Seismic monitoring and analysis of deep geothermal projects in St Gallen and Basel, Switzerland. Geophys J Int 201(2):1022–1039. doi:10.1093/gji/ggv059

Evans KF, Moriya H, Niitsuma H, Jones RH, Phillips WS, Genter A, Sausse J, Jung R, Baria R (2005) Microseismicity and permeability enhancement of hydrogeologic structures during massive fluid injections into granite at 3 km depth at the Soultz HDR site. Geophys J Int 160(1):388–412. doi:10.1111/j.1365-246X.2004.02474.x

Fäh D, Gisler M, Jaggi B, Kästli P, Lutz T, Masciadri V, Matt C, Mayer-Rosa D, Rippmann D, Schwarz-Zanetti G, Tauber J, Wenk T (2009) The 1356 Basel earthquake: an interdisciplinary revision. Geophys J Int 178(1):351–374. doi:10.1111/j.1365-246X.2009.04130.x

Farahbod AM, Kao H, Walker DM, Cassidy JF (2015) Investigation of regional seismicity before and after hydraulic fracturing in the Horn River Basin, Northeast British Columbia. Can J Earth Sci 52(2):112–122. doi:10.1139/cjes-2014-0162

Forghani-Arani F, Behura J, Haines SS, Batzle M (2013) An automated cross-correlation based event detection technique and its application to a surface passive data set. Geophys Prospect 61(4):778–787. doi:10.1111/1365-2478.12033

GeORG Project Team (2013) Geopotenziale des tieferen Untergrundes im Oberrheingraben. LGRB-Informationen 28, Fachlich-Technischer Abschlussbericht des INTERREG-Projekts GeORG, Teil 1. (in German)

Gibbons S, Ringdal F (2012) Seismic monitoring of the North Korea nuclear test site using a multichannel correlation detector. IEEE Trans Geosci Remote Sens 50(5):1897–1909. doi:10.1109/TGRS.2011.2170429

Gibbons SJ, Ringdal F (2006) The detection of low magnitude seismic events using array-based waveform correlation. Geophys J Int 165(1):149–166. doi:10.1111/j.1365-246X.2006.02865.x

Groos JC, Ritter JR (2014) Verbundprojekt MAGS - Konzepte zur Begrenzung der mikroseismischen Aktivität bei der energetischen Nutzung geothermischer Systeme im tiefen Untergrund, Einzelprojekt 1: Quantifizierung und Charakterisierung des induzierten seismischen Volumens im Bereich Landau / Südpfalz. Tech. rep., Karlsruher Institut für Technologie, Final Report of the Project MAGS. in German

Groos JC, Fritschen R, Ritter JR (2013) Untersuchung induzierter Erdbeben hinsichtlich ihrer Spürbarkeit und eventueller Schadenswirkung anhand DIN 4150. Bauingenieur:88. in German

Grund M, Groos JC, Ritter JRR (2016) Fault reactivation analysis using microearthquake clustering based on signal-to-noise weighted waveform similarity. Pure Appl Geophys:1–31. doi:10.1007/s00024-016-1281-4

Grünthal G, Wahlström R (2012) The european-mediterranean earthquake catalogue (EMEC) for the last millennium. J Seismol 16(3):535–570. doi:10.1007/s10950-012-9302-y

Hanka W, Saul J, Weber B, Becker J, Team GITEWS (2008) Timely regional tsunami warning and rapid global earthquake monitoring. Orfeus newsletter:8

Häring M, Schanz U, Ladner F, Dyer B (2008) Characterisation of the Basel 1 enhanced geothermal system. Geothermics 37(5):469–495. doi:10.1016/j.geothermics.2008.06.002

Harris DB, Paik T (2006) Subspace detectors: Efficient implementation. Tech rep. lawrence Livermore National Laboratory, United States

Heimlich C, Gourmelen N, Masson F, Schmittbuhl J, Kim SW, Azzola J (2015) Uplift around the geothermal power plant of Landau (Germany) as observed by InSAR monitoring. Geotherm Energy 3(1):2. doi:10.1186/s40517-014-0024-y

Hettkamp T, Baumgärtner J, Teza D, Lerch C (2013) Experiences from 5 years operation in Landau. In: BESTEC GmbH (ed) Review, Third European Geothermal, Papers and Abstracts, p 23

Holland AA (2013) Earthquakes triggered by hydraulic fracturing in south-central Oklahoma. Bull Seismol Soc Am 103(3):1784–1792. doi:10.1785/0120120109

Illies J (1972) The Rhine Graben rift system-plate tectonics and transform faulting. Geophys Surv 1(1):27–60. doi:10.1007/BF01449550

Joswig M (1990) Pattern recognition for earthquake detection. Bull Seismol Soc Am 80(1):170–186

Kraft T, Mai P, Wiemer S, Deichmann N, Ripperger J, Kästli P, Bachmann C, Fäh D, Wössner J, Giardini D (2009) Enhanced geothermal systems: Mitigating risk in urban areas. Eos 90(32):273–274. doi:10.1029/2009EO320001

Kubacki T, Koper KD, Pankow KL, McCarter MK (2014) Changes in mining-induced seismicity before and after the 2007 Crandall Canyon mine collapse. J Geophys Res Solid Earth 119(6):4876–4889. doi:10.1002/2014JB011037

Landesamt für Geologie und Bergbau Rheinland-Pfalz (2015) Homepage of the Landesamt für Geologie und Bergbau Rheinland-pfalz. www.lgb-rlp.de, accessed 08 May 2015

Lee W, Bennet R, Meaghu K (1972) A method of estimating magnitude of local earthquakes from signal duration. Tech rep., US Geological Survey, USGS Open File Report

Leydecker G (2011) Erdbebenkatalog für Deutschland mit Randgebieten für die Jahre 800 bis 2008 (Earthquake catalogue for Germany and adjacent areas for the years 800 to 2008). Geologisches Jahrbuch:1–198. in German

Ohrnberger M (2001) Continuous automatic classification of seismic signals of volcanic origin at Mt. Merapi, Java, Indonesia. Ph.D. Thesis, Math.-Naturwissenschaftliche Fakulatät der Univ, Potsdam, Germany

Plenkers K, Ritter JR, Schindler M (2013) Low signal-to-noise event detection based on waveform stacking and cross-correlation: application to a stimulation experiment. J Seismol 17(1):27–49. doi:10.1007/s10950-012-9284-9

Richards PG, Waldhauser F, Schaff D, Kim WY (2006) The applicability of modern methods of earthquake location. Pure Appl Geophys 163(2-3):351–372. doi:10.1007/s00024-005-0019-5

Richter CF (1935) An instrumental earthquake-magnitude scale. Bull Seismol Soc Am 25(1):1–32

Rubinstein JL, Ellsworth WL (2010) Precise estimation of repeating earthquake moment: Example from Parkfield, California. Bull Seismol Soc Am 100(5A):1952–1961. doi:10.1785/0120100007

Schaff DP (2010) Improvements to detection capability by cross-correlating for similar events: a case study of the 1999 Xiuyan, China, sequence and synthetic sensitivity tests. Geophys J Int 180(2):829–846. doi:10.1111/j.1365-246X.2009.04446.x

Schaff DP, Richards PG (2011) On finding and using repeating seismic events in and near China. J Geophys Res Solid Earth 116:b03309. doi:10.1029/2010JB007895

Schaff DP, Richards PG (2014) Improvements in magnitude precision, using the statistics of relative amplitudes measured by cross correlation. Geophys J Int 197(1):335–350. doi:10.1093/gji/ggt433

Schaff DP, Waldhauser F (2010) One magnitude unit reduction in detection threshold by cross correlation applied to Parkfield (California) and China seismicity. Bull Seismol Soc Am 100(6):3224–3238. doi:10.1785/0120100042

Shapiro SA, Dinske C, Kummerow J (2007) Probability of a given-magnitude earthquake induced by a fluid injection. Geophys Res Lett 34(22). doi:10.1029/2007GL031615

Shelly DR, Beroza GC, Ide S (2007) Non-volcanic tremor and low-frequency earthquake swarms. Nature 446:305–307. doi:10.1038/nature05666

Skoumal RJ, Brudzinski MR, Currie BS, Levy J (2014) Optimizing multi-station earthquake template matching through re-examination of the Youngstown, Ohio, sequence. Earth Planet Sci Lett 405(0):274–280. doi:10.1016/j.epsl.2014.08.033

Slinkard ME, Carr DB, Young CJ (2013) Applying waveform correlation to three aftershock sequences. Bull Seismol Soc Am 103(2A):675–693. doi:10.1785/0120120058

Song F, Kuleli HS, Toksoez MN, Ay E, Zhang H (2010) An improved method for hydrofracture-induced microseismic event detection and phase picking. Geophysics 75(6):A47–A52. doi:10.1190/1.3484716

Stange S (2006) M_L determination for local and regional events using a sparse network in Southwestern Germany. J Seismol 10(2):247–257. doi:10.1007/s10950-006-9010-6

Walsh FR, Zoback MD (2015) Oklahoma's recent earthquakes and saltwater disposal. Sci Adv 1(5). doi:10.1126/sciadv.1500195

Weingarten M, Ge S, Godt JW, Bekins BA, Rubinstein JL (2015) High-rate injection is associated with the increase in u.s. mid-continent seismicity. Science 348(6241):1336–1340. doi:10.1126/science.aab1345

Withers M, Aster R, Young C (1999) An automated local and regional seismic event detection and location system using waveform correlation. Bull Seismol Soc Am 89(3):657–669

Woessner J, Wiemer S (2005) Assessing the quality of earthquake catalogues: Estimating the magnitude of completeness and its uncertainty. Bull Seismol Soc Am 95(2):684–698. doi:10.1785/0120040007

Ziegler PA (1992) European Cenozoic rift system. Tectonophysics, vol 208. geodynamics of rifting, volume 1 Case history studies on rifts: Europe and Asia